

OPEN

Prion protein modulates endothelial to mesenchyme-like transition in trabecular meshwork cells: Implications for primary open angle glaucoma

Ajay Ashok¹, Min H. Kang², Aaron S. Wise¹, P. Pattabiraman², William M. Johnson³, Michael Lonigro¹, Ranjana Ravikumar¹, Douglas J. Rhee² & Neena Singh¹

Endothelial-to-mesenchyme-like transition (Endo-MT) of trabecular meshwork (TM) cells is known to be associated with primary open angle glaucoma (POAG). Here, we investigated whether the prion protein (PrP^C), a neuronal protein known to modulate epithelial-to-mesenchymal transition in a variety of cell types, is expressed in the TM, and plays a similar role at this site. Using a combination of primary human TM cells and human, bovine, and PrP-knock-out (PrP^{-/-}) mouse models, we demonstrate that PrP^C is expressed in the TM of all three species, including endothelial cells lining the Schlemm's canal. Silencing of PrP^C in primary human TM cells induces aggregation of β 1-integrin and upregulation of α -smooth muscle actin, fibronectin, collagen 1A, vimentin, and laminin, suggestive of transition to a mesenchyme-like phenotype. Remarkably, intraocular pressure is significantly elevated in PrP^{-/-} mice relative to wild-type controls, suggesting reduced pliability of the extracellular matrix and increased resistance to aqueous outflow in the absence of PrP^C. Since PrP^C is cleaved by members of the disintegrin and matrix-metalloprotease family that are increased in the aqueous humor of POAG arising from a variety of conditions, it is likely that concomitant cleavage of PrP^C exaggerates and confounds the pathology by inducing Endo-MT-like changes in the TM.

Prion protein (PrP^C) is a cell surface glycoprotein known mostly for its obligate role in the pathogenesis of prion disorders, a group of neurodegenerative conditions characterized by extensive degeneration of the brain parenchyma and the neuroretina. The key pathogenic event in all prion disorders is a change in the conformation of PrP^C to a β -sheet rich PrP^{Sc} isoform¹⁻³. The resulting loss of function of PrP^C combined with gain of toxic function by PrP^{Sc} are believed to contribute to disease-associated pathology⁴. In support of the loss of function hypothesis, recent reports suggest that dysfunction of PrP^C impairs its ability to fine-tune the Ras homolog gene family member A (RhoA)-associated coiled-coil containing kinase (ROCK) signaling pathway, resulting in over-activation of ROCK and signaling through the LIMK-cofilin pathway^{5,6}. Deletion of PrP in knock-out (PrP^{-/-}) mice or silencing in neuronal cells produces a similar outcome, supporting a key role of PrP^C in regulating cytoskeletal homeostasis^{7,8}. PrP^C also interacts with several extracellular matrix (ECM) proteins⁹, and its absence or altered function induces cell-ECM dyshomeostasis, resulting in loss of neuronal polarity and axonal degeneration in diseased brains^{5,7,10}.

One of the principal outcomes of RhoA-ROCK activation is a shift from cell-cell interactions to cell-substrate interactions, a key event in PrP^C-mediated epithelial to mesenchymal transition (EMT) in several cell types^{8,11}. Trabecular meshwork cells also respond to RhoA-ROCK activation, and upregulate fibrillogenic proteins that deposit in the extracellular matrix (ECM) and increase its stiffness¹²⁻¹⁴. This compromises the response of ECM meshwork to fluctuations in intraocular pressure (IOP) and increases resistance to aqueous outflow, the hallmark

¹Department of Pathology, School of Medicine, Case Western Reserve University, Cleveland, Ohio, 44106, USA.

²Department of Ophthalmology, School of Medicine, Case Western Reserve University, Cleveland, Ohio, 44106, USA.

³Department of Ophthalmology, Duke University, Durham, NC, USA. Correspondence and requests for materials should be addressed to N.S. (email: neena.singh@case.edu)

of primary open angle glaucoma (POAG). Although TM cells do not show the phenotypic changes typical of EMT because of their endothelial nature, the endothelial to mesenchyme-like transition (Endo-MT-like) is sufficient to elevate the IOP and precipitate glaucoma¹⁵. It is encouraging to note that ROCK inhibitors have provided significant benefit in reversing this change, and are promising therapeutic agents for the management of POAG^{16–18}.

While the emphasis on inhibitors of ROCK activation for the therapeutic management of POAG is well-placed, it is equally important to identify pathways upstream or parallel to RhoA-ROCK, and cross-talk between different pathways. Examples include signaling through integrins^{19–21}, TGF β ^{21,22}, autotaxin-LPA²³, JNK-paxillin²⁴, and cross-talk between TGF β , integrins, and the ECM²⁵ to name a few. An additional possible player is PrP^C, a documented inducer of EMT through β 1-integrin and RhoA-ROCK activation^{5,7,11,26}. This question deserves attention because PrP^C is cleaved by members of the disintegrin and matrix-metalloprotease family of enzymes that are upregulated in the aqueous humor (AH) of glaucomatous eyes^{27,28}, and is likely to confound the pathogenesis and therapeutic management of POAG through cross-talk with other pathways²⁹.

Here, we explored the expression and functional significance of PrP^C in the TM of human, bovine, and mouse eyes. We demonstrate that PrP^C is expressed in the TM of all three species, and plays a significant role in maintaining the ECM structure at this site. In addition, significant amounts of soluble PrP^C are present in the AH, suggesting constitutive or regulated shedding of membrane-bound PrP^C in the anterior segment³⁰.

Results

Expression of PrP^C in human, bovine, and murine trabecular meshwork. Immunoreaction of human TM sections for PrP^C showed strong reaction in all layers of the TM (Fig. 1a, panels 1 & 2). Reaction with mouse IgG and H&E staining of serial sections confirmed the specificity of the immunoreaction and accurate identification of the TM region (Fig. 1a, panels 3 & 4). A similar evaluation of non-permeabilized primary human TM cells revealed expression of PrP^C on the plasma membrane as in neuronal and other cells (Fig. 1b, panel 1, arrowheads)³¹. No reaction was detected with non-specific mouse IgG processed in parallel (Fig. 1b, panel 2).

Further confirmation of the above results was obtained by performing a similar analysis on bovine and mouse TM tissue (Fig. 2). Immunoreaction of fixed bovine TM sections for PrP^C revealed strong reactivity on the plasma membrane of TM cells and endothelial cells of the aqueous plexus (AP) (Fig. 2a panel 1, arrowheads)³². No reaction was detected in a serial section reacted with non-specific mouse IgG (Fig. 2a, panel 2). A similar evaluation of mouse TM sections showed strong reactivity for PrP^C in PrP^{+/+}, and complete absence in PrP^{-/-} sections as expected (Fig. 2b, panels 1 & 2). Serial sections from the same block reacted with mouse IgG showed no reactivity (Fig. 2b panel 3). H&E staining confirmed accurate identification of the TM region in PrP^{+/+} sections of the anterior segment (Fig. 2b, panel 4).

Processing of PrP^C in human ocular tissues. To evaluate the expression and processing of PrP^C in different regions of the eye, antibodies spanning the entire sequence of PrP^C were used (Fig. 3a). Thus, lysates of primary human TM cells were evaluated as such, or deglycosylated before processing for Western blotting. Probing of lysates with 3F4 that reacts with full-length (FL) and β -cleaved PrP^C showed glycosylated and unglycosylated forms as expected (Fig. 3b, lanes 1–3). However, deglycosylation with PNGase-F revealed that 30–50% of FL PrP^C (#, 27 kDa) was cleaved at the β -site (C2, white arrowhead, 20 kDa) (Fig. 3b, lanes 4–6; Fig. 3f). No reaction was detected in samples from TM cells transfected with PrP^C-specific siRNA (Fig. 3b, lane 7). Lysate from human brain was fractionated in parallel as a positive control (Fig. 3b, lane 8). Re-probing with 8H4 showed α -cleaved 18 kDa band (C1, *), representing a minor fraction of the total (Fig. 3b, lanes 12–14). No reactivity was detected in samples treated with PrP^C-specific siRNA (Fig. 3b, lane 15).

Evaluation of tissue from different regions of the human eye with 8H4 showed strong reactivity for FL PrP^C in the TM, retina (Ret), optic nerve (ON), and ciliary body (CB) (Fig. 3c, lanes 1–4, #). However, the presence of a unique 19 kDa band in the ON was surprising (Fig. 3c, lane 3), prompting additional exploration.

To achieve this goal, three pairs of human eyes were dissected to isolate the TM, CB, retina, and ON, and tissue homogenates were evaluated as such or deglycosylated before Western blotting. Lysate from human brain was fractionated in parallel as a positive control. To avoid experimental artifacts, membranes probed once with a particular PrP^C-specific antibody were re-probed only for β -actin, not with another PrP antibody.

Probing of lysates from the TM and CB with 8B4 that reacts with FL and N-terminal fragments of α - and β -cleaved PrP were not detected because these are soluble and unlikely to be present in significant amounts in tissue lysates³³. Probing with 3F4 showed mainly β -cleaved PrP^C (Fig. 3d, lanes 7–10, white arrowhead). Reaction with G-12, a C-terminal antibody that reacts with FL, β -cleaved, α -cleaved, and probably γ -cleaved soluble FL PrP^C showed mainly β -cleaved PrP^C in the TM, and α -cleaved fragment in the CB and brain samples (Fig. 3d, lanes 13–18, white arrowhead, *). Similar results were obtained with 2301, validating the results with G-12 (Supplementary Fig S3). In bovine CB, however, PrP^C showed equivalent representation of α - and β -cleaved forms³⁰, suggesting species-specific differences in its proteolytic processing.

Lysates from ON and retina showed FL and α -cleaved PrP^C (Fig. 3e, lanes 1–18, #, *). The retina also showed β -cleaved PrP^C (Fig. 3e, lanes 6, 12, and 18, white arrowhead). Surprisingly, the optic nerve showed a unique fragment of ~19 kDa that reacted with the N-terminal antibody 8B4 (Fig. 3e, lane 2, ?). This fragment also reacted with 8H4 (Fig. 3c, lane 3) and 3F4 (Fig. 3e, lane 14), but not with 2301 (Fig. 3e, lane 16). These observations suggest that this fragment is distinct from α , β , and γ -cleaved PrP^C for the following reasons; (1) it is glycosylated and hence includes at least one N-glycan (amino acid 175) (Fig. 3e, lanes 1 & 2, lanes 13 & 14), (2) it reacts with 8B4, suggesting the presence of N-terminal amino acid 35 (Fig. 3a), (3) it does not react with 2301 (Fig. 3a), and (4) migrates at ~19 kDa, a molecular mass that is inconsistent with γ -cleaved or FL PrP^C. Further exploration is necessary to characterize this fragment fully and understand the conditions that precipitate its cleavage.

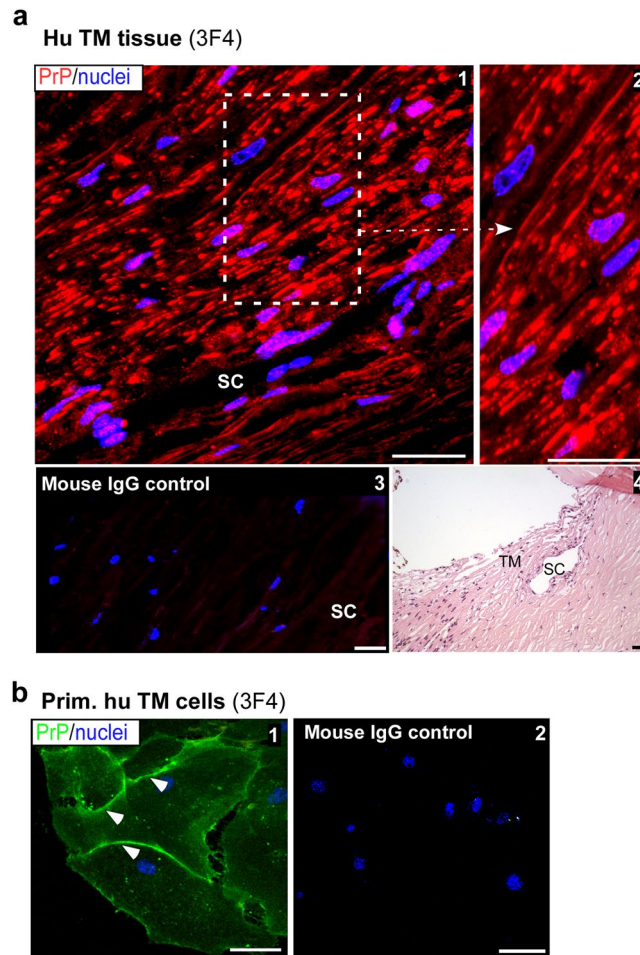


Figure 1. Distribution of PrP^C in the human trabecular meshwork. **(a)** Immunoreaction of human TM section with PrP-specific antibody 3F4 followed by Alexa fluor 546-conjugated secondary antibody shows strong reactivity in all layers of the TM (panel 1). High magnification image demonstrates expression of PrP^C on the plasma membrane of TM cells (panel 2). A serial section reacted with mouse IgG and Alexa fluor 546-conjugated secondary antibody shows no reaction (panel 3). H&E staining of a serial section confirms the TM region and Schlemm's canal (SC) (panel 4). Scale bar: 25 μm. **(b)** Non-permeabilized primary human TM cells reacted with 3F4 followed by Alexa Fluor 488-conjugated secondary antibody show expression of PrP^C on the plasma membrane (panel 1). No reaction is detected in control cells exposed to mouse IgG followed by the same secondary antibody (panel 2). Scale bar: 25 μm.

Quantification of relative abundance of FL, C1 (α-cleaved), and C2 (β-cleaved) forms of PrP^C in different tissues showed a ratio of 32:6:62 for TM cells, 9:27:64 for TM tissue, 20:60:20 for CB, 30:35:5:30 (unique) for optic nerve, and 14:45:41 for the retina (Fig. 3f). These ratios are an approximation at best because of the efficiency of reactivity of different antibodies. However, it is clear that unlike brain and neuronal cells where 60–70% of PrP^C is cleaved at the α-site, processing of PrP^C in ocular tissues is distinct, and is mainly at the β-site in human TM tissue.

Silencing of PrP^C induces mesenchyme-like transition in the TM. Absence of PrP^C has been reported to induce aggregation of β1-integrin in neuronal cells⁸, triggering the Rho/ROCK pathway. To evaluate if a similar process occurs in the TM, primary human TM cells were transfected with PrP-specific siRNA, and non-permeabilized cells were immunoreacted with antibody specific for activated β1-integrin. Downregulation of PrP^C resulted in clustering of β1-integrin on the plasma membrane as opposed to control cells that showed uniform distribution (Fig. 4a, panels 1–4, arrowheads). Control cells where the primary antibody was omitted did not show any reaction (Fig. 4a, panel 5). Western blotting of lysates did not show a significant difference in β1-integrin expression levels as reported in a previous study⁹ (Supplementary Fig. S4).

To evaluate whether clustering of β1-integrin activates downstream pathways resulting in Endo-MT-like transition, primary human TM cells were transfected with PrP-specific siRNA to downregulate PrP^C, and the expression and distribution of fibrillogenic proteins indicative of Endo-MT-like transition was evaluated by Western blotting.

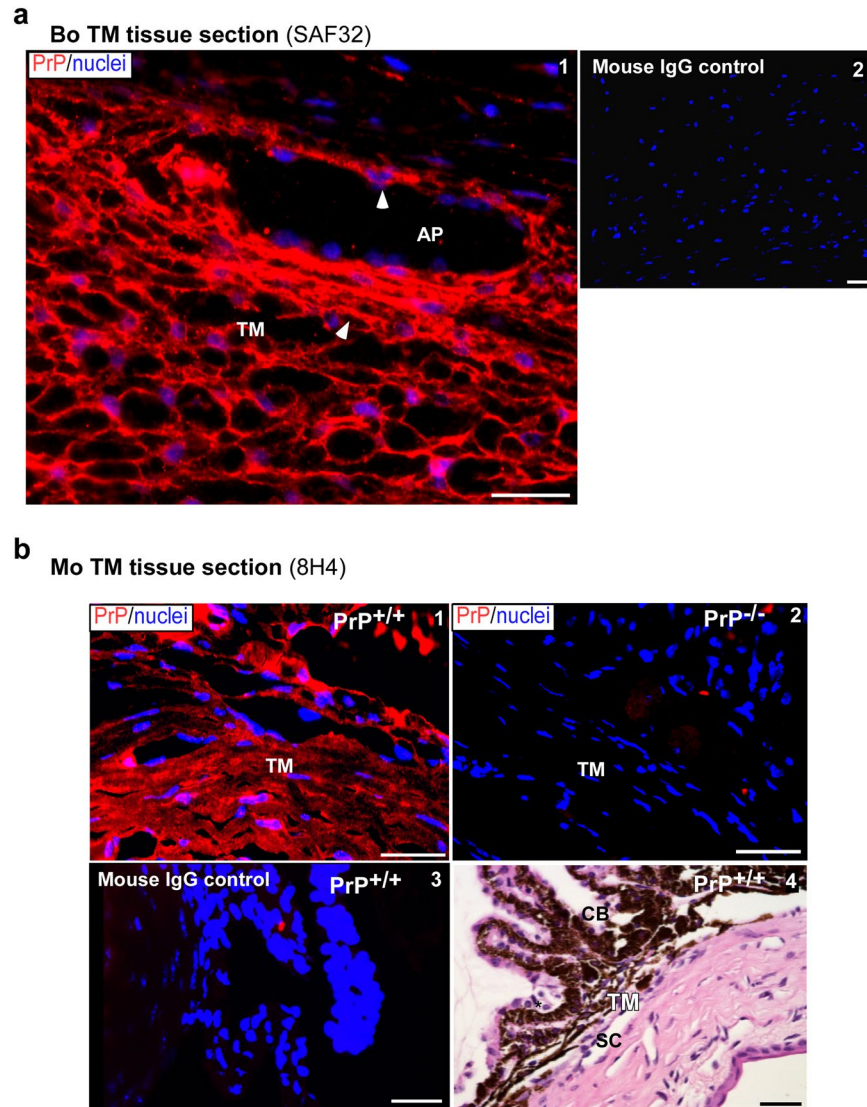


Figure 2. Expression of PrP^C in bovine and murine TM. (a) Immunoreaction of bovine TM section with PrP-specific antibody SAF32 followed by Alexa fluor 546-conjugated secondary antibody shows strong reactivity for PrP^C on the plasma membrane of TM cells and endothelial cells lining the aqueous plexus (AP) (panel 1, arrowhead). No reaction is detected in a serial section exposed to mouse IgG followed by the same secondary antibody (panel 2). Scale bar: 25 μ m. (b) Immunoreaction of the anterior segment of PrP^{+/+} mouse eye with PrP-specific antibody 8H4 followed by Alexa fluor 546-conjugated secondary antibody shows expression of PrP^C in all layers of the TM (panel 1). No reaction is noted in PrP^{-/-} mouse sample processed in parallel (panel 2). Reaction of PrP^{+/+} sample with mouse IgG followed by the same secondary antibody shows no reaction (panel 3). H&E staining of a serial section confirms accurate identification of the TM region (panel 4). Scale bar: 25 μ m.

Probing for PrP^C revealed the expected glycoforms in cells transfected with scrambled siRNA, and >98% downregulation by PrP-specific siRNA (Fig. 4b, lanes 1 & 2). Probing for laminin and laminin receptor (LR) showed significant upregulation in the absence of PrP^C relative to controls (Fig. 4b, lanes 1 & 2; Fig. 4c). Immunoreaction of control and experimental cells for laminin and laminin-receptor confirmed the immunoblotting results (Supplementary Fig. S5).

A similar evaluation of duplicate cultures showed significant downregulation of PrP^C by siRNA treatment as above (Fig. 5a, lanes 1 & 2). Notably, downregulation of PrP^C resulted in significant upregulation of α -smooth muscle actin (α -SMA) and fibronectin relative to controls (Fig. 5b, lanes 1 & 2; Fig. 5c). Immunostaining of sections from PrP^{-/-} and PrP^{+/+} mouse eyes for α -SMA and fibronectin showed more reaction in the TM of PrP^{-/-} relative to PrP^{+/+} controls (Fig. 5d & 5e, panels 1–4), supporting the above results. Immunoreaction with mouse IgG showed no reaction (Fig. 5d, panels 5 & 6).

Further probing of lysates from human TM cells transfected with scrambled and PrP-siRNA showed significant upregulation of vimentin and collagen 1A by downregulation of PrP^C in comparison to controls (Fig. 6a, lanes 1 & 2; Fig. 6b). Immunostaining of sections from the anterior segment of PrP^{-/-} and PrP^{+/+} mouse eyes for vimentin and collagen 1A showed more reactivity in PrP^{-/-} relative to PrP^{+/+} samples (Fig. 6c,d, panels 1–4),

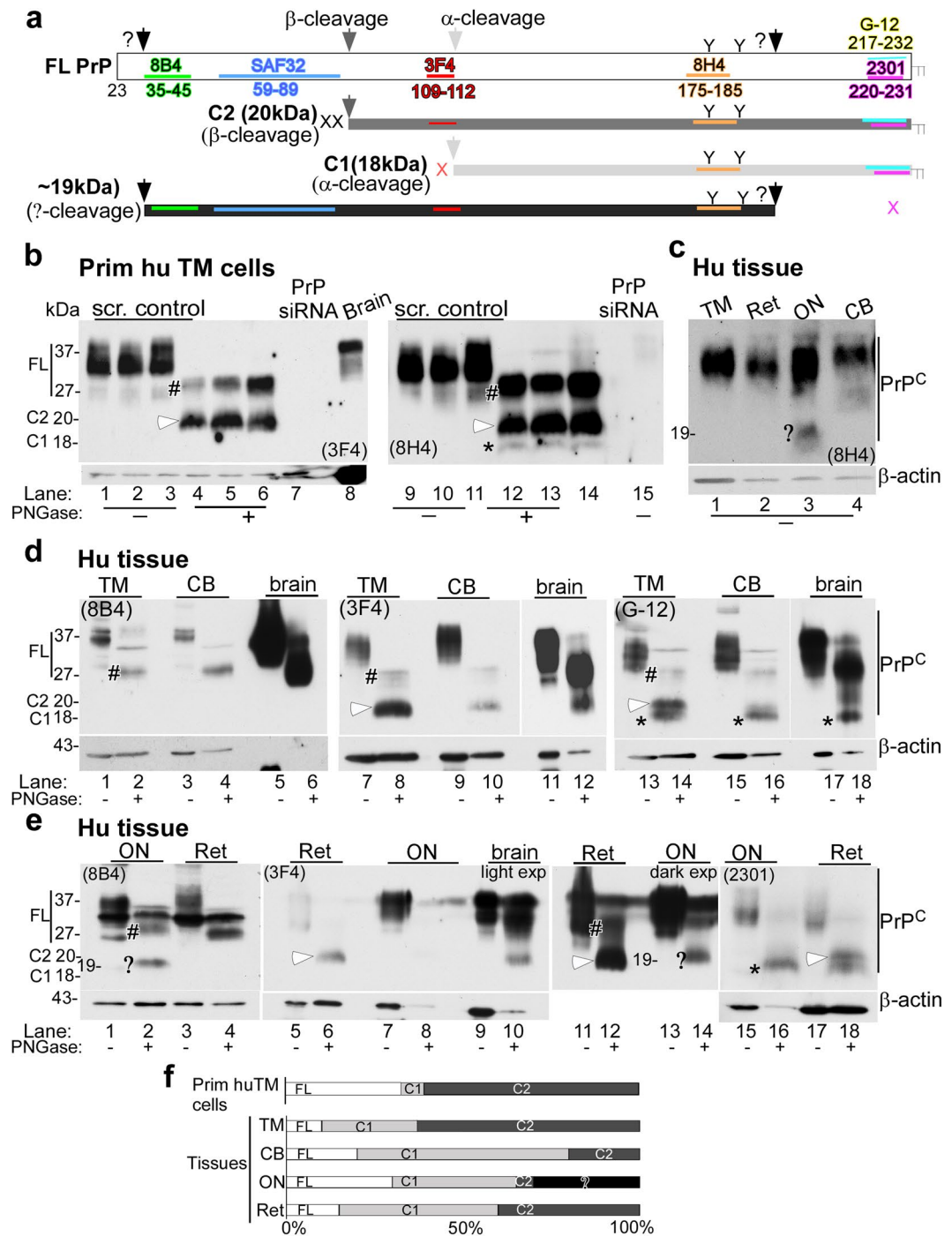


Figure 3. Processing of PrP^C in human ocular tissue. **(a)** Schematic representation of full length (FL), α-cleaved (C1, 18 kDa), β-cleaved (C2, 20 kDa), and ~19 kDa forms of PrP^C. Antibody 8B4 reacts with FL and N-terminal fragments of PrP^C, 3F4 reacts with FL and C2, and 8H4, G-12, and 2301 react with FL, C1, and C2. **(b)** Probing of lysates from primary human TM cells cultured from three different cases with 3F4 and 8H4 shows FL and mainly C2 fragment of PrP^C. C1 represents a small fraction of total PrP^C. Human brain lysate provides a positive control, and lysates from cells transfected with PrP-siRNA serve as a negative control (lanes 1–15). **(c)** Probing of lysates from the TM, retina (Ret), optic nerve (ON), and CB with 8H4 shows glycosylated PrP^C in all samples (lanes 1–4), and a ~19 kDa fragment in lysates from the ON (lane 3,?) **(d)** Probing of human TM and CB lysates with 8B4, 3F4, and G-12 shows FL glycosylated and deglycosylated PrP^C in all samples as in human brain. The TM shows significantly more C2 relative to FL and C1, while the brain shows mainly FL and a small amount of C1 (lanes 1–18) (lighter exposures are shown for lanes 11 and 12. Complete membrane is shown in Supplementary Fig. S2). TM and CB lysates probed with 2301 antibody mimicked the G-12 probing data (Supplementary Fig. S3) **(e)** Probing of lysates from the ON and retina with 8B4, 3F4, and 2301 shows FL PrP^C as in human brain, and a ~19 kDa fragment in deglycosylated ON sample. The retina has significantly more C2 relative to FL and C1, while the ON has more C1 relative to C2. The ~19 kDa fragment

does not react with 2301 (lanes 15–18). (FL: #; C1: star; C2: white arrowhead; ~19 kDa). All membranes were re-probed for β -actin to control for loading. (f) The relative abundance of FL, C1, C2, and the ~19 kDa fragment is shown graphically. Figures 3c–e are from tissue harvested from the same eye. Similar results were obtained from two other eye globes.

supporting the results from primary human TM cells. Immunoreaction with mouse IgG (for vimentin) and rabbit IgG (for collagen 1A) showed no reaction (Fig. 6c,d, panels 5 & 6).

Together, the above results demonstrate that absence or downregulation of PrP^C in mouse models or in primary human TM cells aggregates β 1-integrin and upregulates fibrillogenic proteins including α -SMA, fibronectin, vimentin, and collagen 1A, the ECM protein laminin, and surprisingly, also the receptor for laminin.

Absence of PrP^C upregulates myocilin. Myocilin is a biomarker for TM cells, and is upregulated by dexamethasone treatment³⁴. Since human TM cells are likely to change their morphology in culture, dexamethasone-mediated upregulation of myocilin, a reliable method for their validation³⁵, was used before every experiment (Fig. 7a, lanes 1 & 2; Fig. 7b). Surprisingly, downregulation of PrP^C also upregulated myocilin in primary human TM cells (Fig. 7a, lane 1 vs. 3; Fig. 7b), and blunted their response to dexamethasone (Fig. 7a, lane 1 vs 3 & 4; Fig. 7b). Probing for PrP^C showed the expected glycoforms in cells treated with scrambled siRNA as expected, and almost complete absence in cells transfected with PrP-siRNA (Fig. 7a, lanes 1–4).

Immunoreaction of mouse TM sections for myocilin revealed significantly stronger reactivity in PrP^{-/-} samples relative to PrP^{+/+} controls (Fig. 7c, panels 1 & 2), confirming the results from human TM cells. Immunoreaction with mouse IgG showed no reactivity (Fig. 7c panel 3).

Absence of PrP^C elevates intraocular pressure. To establish the clinical relevance of our observations to POAG, age and sex-matched PrP^{+/+} and PrP^{-/-} mice were anesthetized, and IOP was measured in both eyes with a tonometer. To eliminate bias, measurements were performed in separate sets of mice by three different individuals blinded to the mouse genotype. Surprisingly, IOP was significantly elevated in PrP^{-/-} eyes relative to PrP^{+/+} controls (Fig. 7d). The increase in IOP in PrP^{-/-} mice is in good agreement with upregulation of fibrillogenic proteins^{36,37}, the hallmark of altered cell-ECM interactions in the TM.

Discussion

We report that PrP^C is expressed in the TM, and modulates cell-ECM interactions at this site. Downregulation of PrP^C in primary human TM cells induced aggregation of β 1-integrin on the plasma membrane and upregulation of fibrillogenic proteins. Likewise, fibrillogenic proteins were upregulated in the TM of PrP^{-/-} mice, indicating an Endo-MT-like transition. *In vivo* measurement of IOP revealed significant elevation in PrP^{-/-} relative to PrP^{+/+} mouse eyes, implicating PrP^C in the pathophysiology of POAG.

Our data demonstrate expression of PrP^C in the TM of human, bovine and mouse eyes, including endothelial cells of the Schlemm's canal and the aqueous plexus (in bovine) that modulate aqueous outflow^{12,38}. In primary human TM cells, PrP^C was detected on the plasma membrane as in neuronal and other cell types. However, unlike neurons where majority of PrP^C is cleaved at the α -site, most of the PrP^C in TM cells was cleaved at the β -site. Unlike α -cleavage that occurs during physiological recycling of PrP^C from the plasma membrane³⁹, β -cleavage is associated with oxidative stress^{40–42}, iron transport^{30,43,44}, conversion of PrP^C to PrP^{Sc1,3}, and possibly other stimuli⁴⁵. It is surprising that human TM, ciliary body, optic nerve, and the retina showed distinct cleavage patterns of PrP^C. In TM cells, TM tissue, and ciliary body, PrP^C was mostly β -cleaved, while in the retina PrP^C showed almost equal representation of α - and β -cleaved forms. Full-length PrP^C was minimal in all of the above ocular tissues. These observations differ from ~50% β -cleavage of PrP^C human retinal pigment epithelial cells⁴⁴, and almost equal representation of α - and β -cleaved PrP^C forms in bovine ciliary body³⁰. Since bovine and human eyes have different concentrations of oxalate, apo-transferrin, and possibly other anti-oxidants that determine susceptibility to light-induced oxidative stress⁴⁶, it is likely that cleavage of PrP^C partly depends on the exposure of a particular ocular region to light or other stimuli that increase oxidative stress. It is notable that the optic nerve showed a novel internal fragment of ~19 kDa that requires further characterization. The soluble N-terminal fragments of α -, β -, and other cleaved forms of PrP^C are likely to accumulate in the AH and vitreous humor and play distinct physiological roles as in neurons⁴⁵, a possibility that is currently under investigation.

The stimuli and the identity of enzymes responsible for the mainly β -cleavage of PrP^C in most ocular tissues and a unique cleavage in the optic nerve is not clear from our data. These are important unanswered questions with significant physiological and pathological implications^{45,47–49}. In neuronal cells, PrP^C undergoes at least four different proteolytic events. α -Cleavage is predominant, and the neuroprotective role of the resultant N-terminal fragment N1 has been described⁴⁵. The proteases responsible for this cleavage, however, are not clear, and are arbitrarily termed α -PrPases^{48,50}. Cleavage near the C-terminus releases almost full-length PrP^C in the extracellular milieu, and is believed to protect neurons by reducing the substrate for PrP-scrapie, the disease-associated isoform of PrP^C, on neuronal cells. Implications of soluble PrP^C in the extracellular milieu, however, are not clear. This cleavage is mediated by the disintegrin and metalloprotease ADAM10^{51–53}. ADAM9 influences ADAM10 activity, and is thus indirectly responsible for this event^{41,42,54}. Additional cleavage of mainly unglycosylated PrP^C near the C-terminus has been described, and is termed γ -cleavage. The responsible protease is probably a member of the matrix metalloprotease family⁴². It is pertinent to mention here that matrix metalloproteases 2 and 9, ADAM proteases 9 and 10, and tetraspanin 6, a member of the tetraspanin family necessary for the maturation and transport of ADAM10, are increased in the AH of glaucomatous eyes of diverse etiology^{27,55,56}. This raises the possibility that shedding of PrP^C from TM cells may induce Endo-MT-like transition and altered TM-ECM interactions, contributing to the ongoing pathology. β -cleavage of PrP^C is mainly associated with pathological

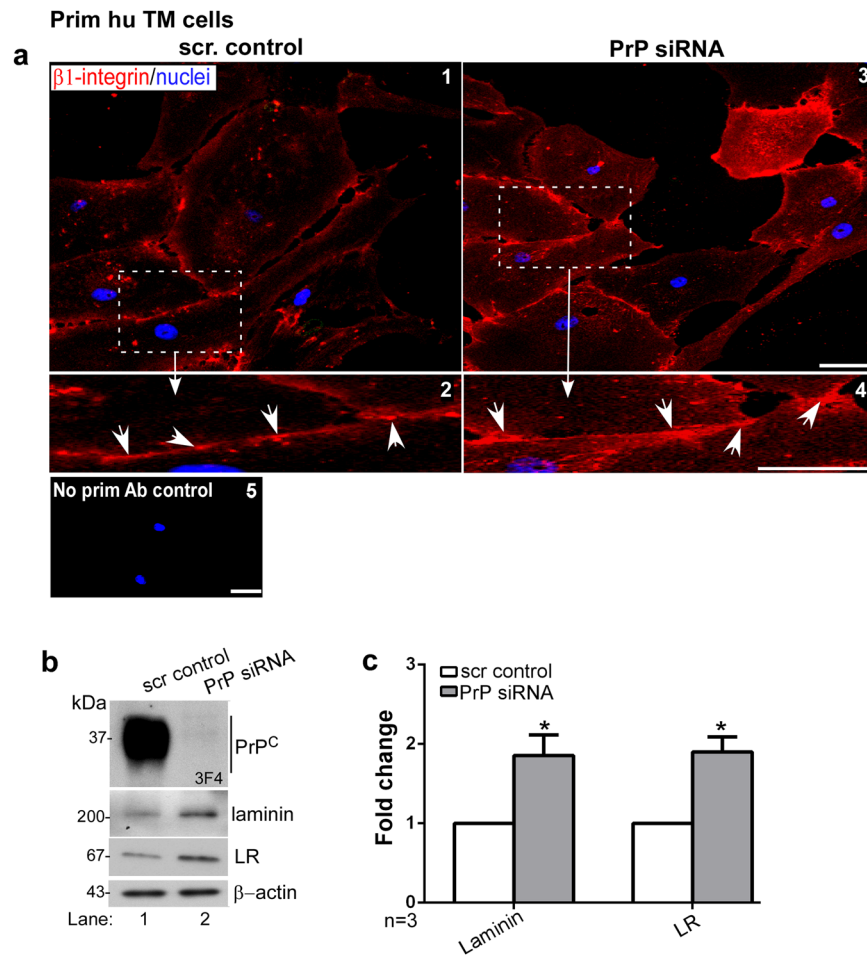


Figure 4. Downregulation of PrP^C aggregates β 1-integrin and upregulates laminin and its receptor. (a) Silencing of PrP^C in human TM cells followed by immunostaining with antibody specific for activated β 1-integrin shows clustering of activated β 1-integrin on the plasma membrane in the absence of PrP^C (arrowheads) (panels 1–4). Cells transfected with PrP-siRNA and reacted with mouse IgG and respective secondary antibody do not show any reaction (panel 5). Scale bar: 25 μ m. (b) Probing of TM cell lysates for PrP^C shows the expected glycoforms in control cells transfected with scrambled siRNA, and minimal reaction in cells exposed to PrP-siRNA (lanes 1 & 2). Probing for laminin and laminin receptor (LR) shows significant upregulation in the absence of PrP^C relative to control (lanes 1 & 2). (c) Quantification by densitometry after normalization with β -actin shows 2-fold upregulation of laminin and LR due to downregulation of PrP^C. Values are mean \pm SEM of the indicated n. * $p < 0.05$. Full-length blots are included in the Supplementary Fig. S2.

conditions, and is mediated by calpains, lysosomal proteases, and oxidative stress. It is believed that the released N-terminal fragment N2 is an anti-oxidant and thus neuroprotective^{45,49,57}. This raises the interesting possibility that β -cleavage of PrP^C is an adaptive response, and increased levels of N2 protect the highly sensitive ocular tissues from light-induced oxidative stress. Further exploration is necessary to understand the physiological and pathological implications of this phenomenon fully.

It is remarkable that downregulation of PrP^C in TM cells caused significant upregulation of several fibrillogenic proteins including α -SMA, fibronectin, and collagen 1A, suggesting transformation to a mesenchyme-like phenotype^{11,13,38,58}. Absence of PrP^C in neuronal cells induces aggregation of β 1-integrin on the plasma membrane, activating signaling pathways including RhoA-ROCK that interfere with neuronal polarity and axonal growth by altering cell-ECM interactions^{5–8,26,59,60}. Our data suggest that a similar mechanism operates in TM cells, and induces upregulation of fibrillogenic proteins typical of the glaucomatous change^{12,15}.

PrP^C is also a cell surface receptor for laminin, an extracellular matrix glycoprotein that plays a major role in neuronal differentiation¹⁰. Deletion or dysfunction of PrP^C causes aggregation and accumulation of laminin in intra- and extracellular compartments and compensatory upregulation of laminin receptor in astrocytes and neuronal cells^{9,10}. Our data show a similar response in TM cells, where upregulation of fibronectin is likely to contribute further to endo-MT-like changes^{12,38}. Upregulation of vimentin upon downregulation of PrP^C suggests loss of adherens junctions, another characteristic of such a change. Since laminin and vimentin are putative ligands of PrP^C³¹, these changes are likely to be independent of ROCK activation, and suggest that PrP^C contributes to Endo-MT-like transition in TM cells by both ROCK-dependent and independent pathways.

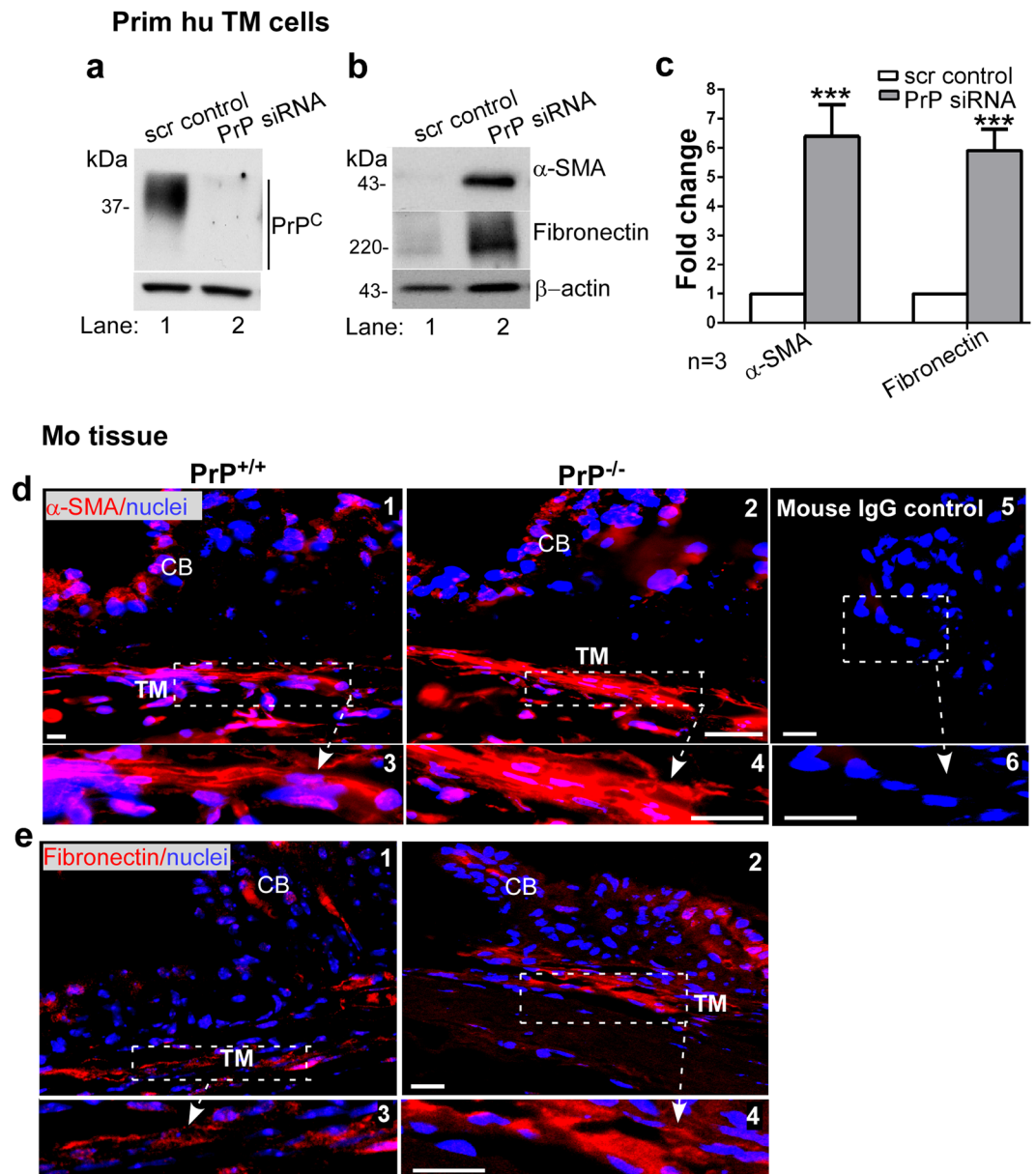


Figure 5. Downregulation of PrP^C upregulates α -SMA and fibronectin in the TM. (a) Probing of TM cell lysates treated with scrambled and PrP-siRNA for PrP^C shows the expected glycoforms in the scrambled control, and minimal reactivity for PrP^C in the experimental sample (lanes 1 & 2). (b) Probing of the same lysates for α -SMA and fibronectin shows upregulation in the absence of PrP^C relative to controls (lanes 1 & 2). (c) Quantification of protein expression by densitometry after normalization with β -actin shows 6.1-fold and 5.9-fold upregulation of α -SMA and fibronectin respectively. Values are mean \pm SEM of the indicated n. * $p < 0.05$, ** $p < 0.01$. Full-length blots (Supplementary Fig. S2). (d & e) Immunoreaction of fixed sections from the anterior segment of PrP^{+/+} and PrP^{-/-} mice shows stronger reactivity for α -SMA and fibronectin in the TM of PrP^{-/-} relative to PrP^{+/+} samples (panel 1 vs. 2). Scale bar: 25 μ m. No reaction was detected in samples reacted with mouse IgG followed by Alexa 546-conjugated secondary antibody (panels 5 & 6).

Upregulation of myocilin due to silencing of PrP^C is difficult to explain from our data. Since exposure to dexamethasone, a known inducer of myocilin did not cause additional upregulation of myocilin in the absence of PrP^C, it is likely that both pathways intersect, perhaps through ROCK activation³⁴. Additional studies are necessary to understand the relationship between PrP^C and myocilin.

In conclusion, this study demonstrates a significant role of PrP^C in maintaining cell-ECM interactions TM, and possibly as an anti-oxidant. Downregulation or absence of PrP^C induces an endo-MT-like transition in the TM and elevation of IOP in PrP^{-/-} mice, typical of POAG (Fig. 8)⁶¹. These observations underscore the significance of PrP^C as a trigger for endo-TM-like transition in TM cells, and its potential to aggravate glaucomatous pathology due to shedding by ADAM and matrix-metalloproteases in the AH of glaucomatous eyes. Future

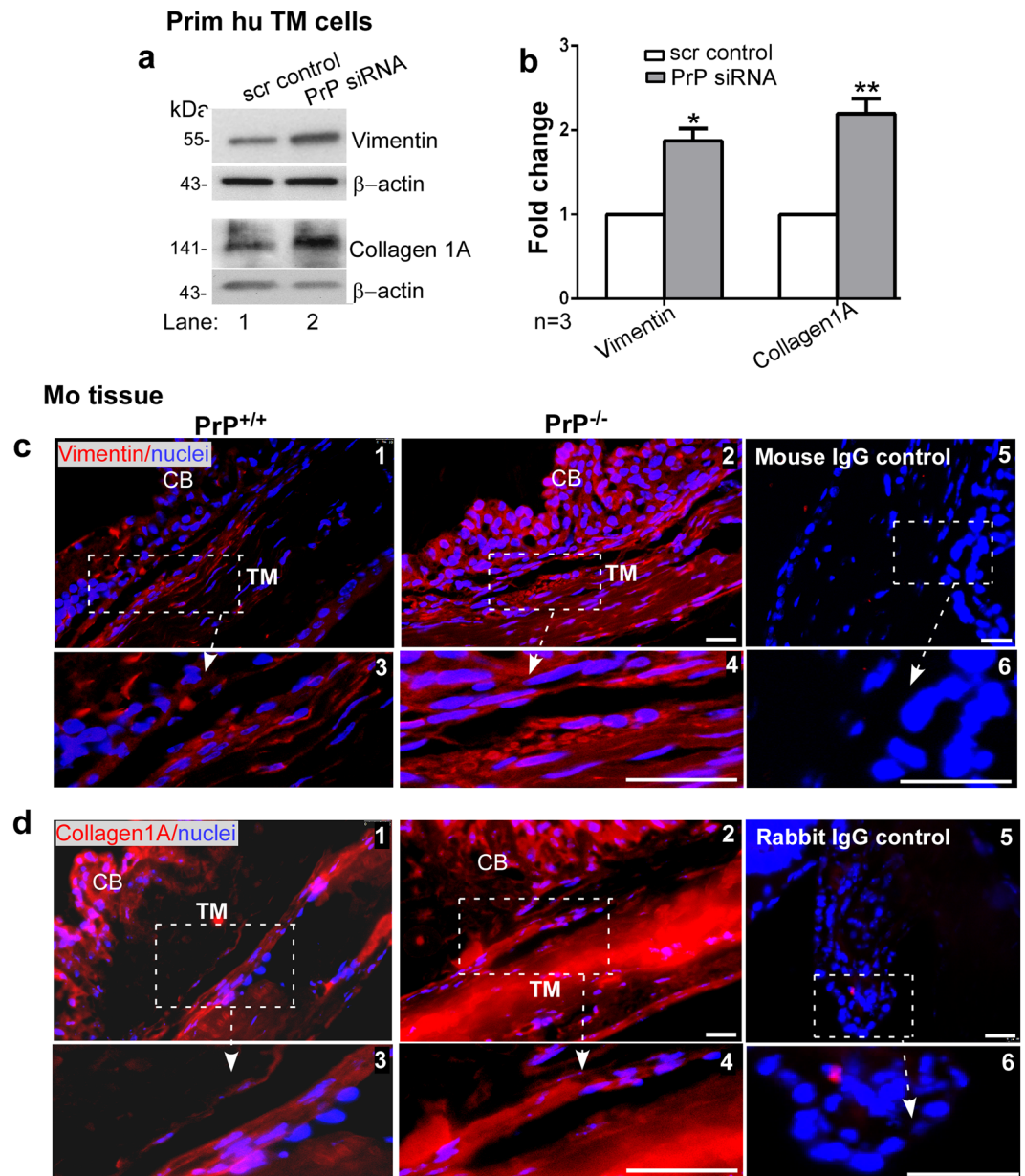


Figure 6. Downregulation of PrP^C upregulates vimentin and collagen 1A. **(a)** PrP^C was silenced in human TM cells and lysates were processed as above. Probing for vimentin and collagen 1A shows significant upregulation in the absence of PrP^C relative to controls (lanes 1 & 2). **(b)** Quantification of protein expression by densitometry after normalization with β -actin shows 1.9-fold upregulation of vimentin and 2.2-fold upregulation of collagen 1A in the absence of PrP^C. Values are mean \pm SEM of the indicated n. * $p < 0.05$, ** $p < 0.01$. Full-length blots (Supplementary Fig. S2). **(c & d)** Immunoreaction of fixed sections from the anterior segment of PrP^{+/+} and PrP^{-/-} mice for vimentin and collagen 1A shows stronger reaction in the TM of PrP^{-/-} relative to PrP^{+/+} samples (panel 1 vs. 2). No reaction was detected when serial sections were reacted with mouse or rabbit IgG followed by Alexa 546-conjugated secondary antibody (panels 5 & 6). Scale bar: 25 μ m.

exploration in additional PrP^{-/-} and over expression mouse models and *ex-vivo* perfusion models of human eye where levels of PrP^C have been altered experimentally are necessary to define its precise role in ocular tissues.

Methods

Ethics statement. All animal procedures were in accordance with the ARVO Statement for the Use of Animals in Ophthalmic and Vision Research. Animal experiments were approved by the Association for Assessment and Accreditation of Laboratory Animal Care International (AAALAC)-approved Animal Resource Center (ARC) at Case Western Reserve University (CWRU) School of Medicine (SOM).

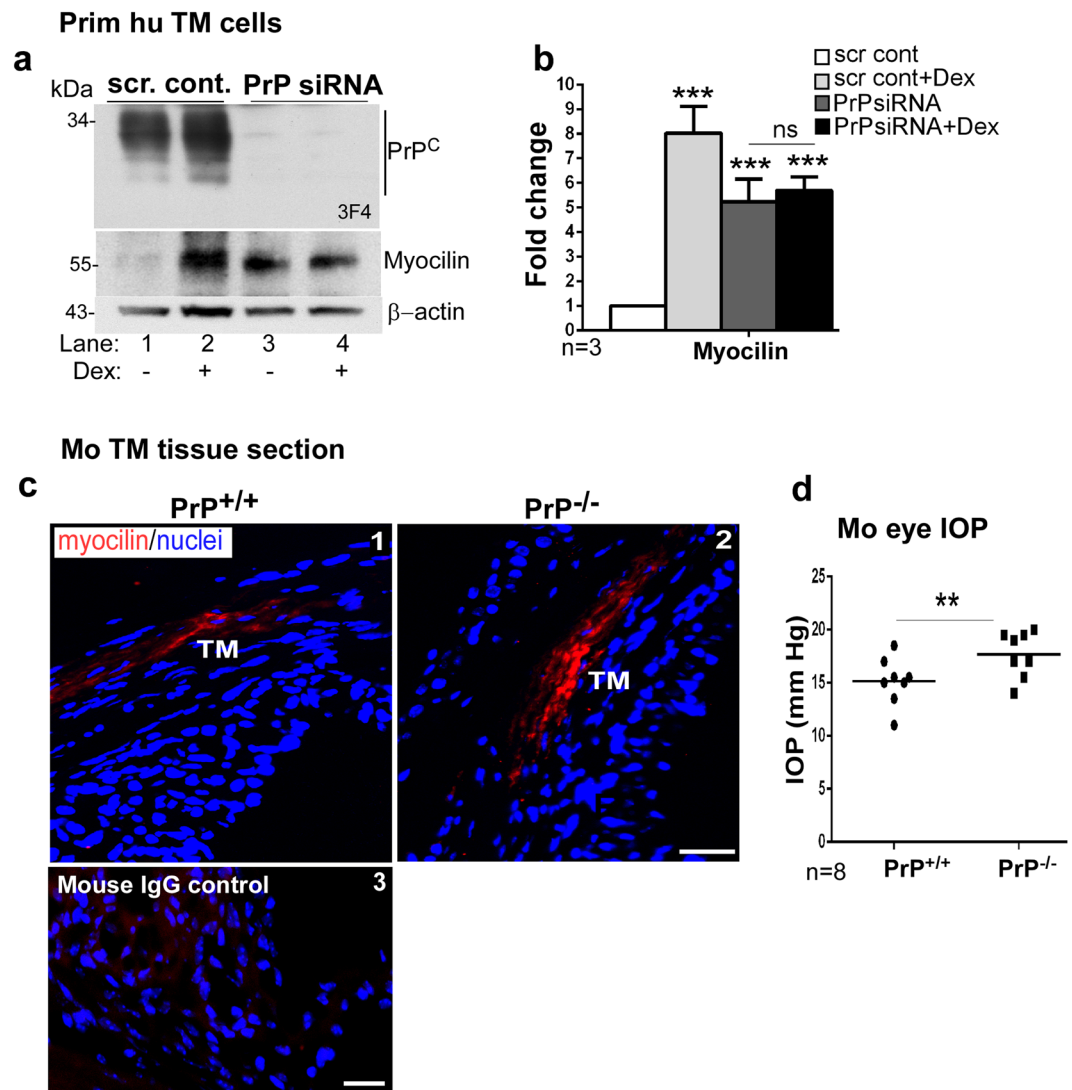


Figure 7. Myocilin is upregulated by downregulation of PrP^C. **(a)** PrP^C was silenced in primary human TM cells and lysates were processed as above. Probing for PrP^C shows the expected glycoforms in controls, and minimal reaction in samples treated with PrP-siRNA (lanes 1 & 2 vs. 3 & 4). Re-probing for myocilin shows significant upregulation in the absence of PrP^C (lane 1 vs 3). Exposure of control and experimental cells to dexamethasone (Dex) shows upregulation of myocilin as expected (lanes 1 & 2). However, no additive effect of dexamethasone is noted in the absence of PrP^C (lanes 3 & 4). **(b)** Quantification by densitometry after normalization with β-actin shows 8-fold upregulation of myocilin by dexamethasone, and ~5.3-fold upregulation in the absence of PrP^C regardless of dexamethasone. Values are mean ± SEM of the indicated n. ***p* < 0.01; ns: not significant. Full-length blots are included in the Supplementary Fig. S2. **(c)** Immunoreaction of anterior segment of PrP^{+/+} and PrP^{-/-} mice for myocilin shows upregulation in the TM of PrP^{-/-} sections relative to controls (panels 1 & 2). No reaction was detected in a serial section reacted with mouse IgG followed by Alexa 546-conjugated secondary antibody (panel 3). Scale bar: 25 μm. **(d)** Measurement of IOP shows significant upregulation in PrP^{-/-} eyes relative to PrP^{+/+} controls (n = 8). Values are mean ± SEM of the indicated n. ***p* < 0.01.

Antibodies and Chemicals. HRP-conjugated secondary antibodies (anti-mouse (NA931V), anti-rabbit (NA92V)) were from GE Healthcare (supplied by Sigma, USA). Alexa Fluor 546 (A11071, A11018) and Alexa Fluor 488 (A11017) tagged secondary antibodies were from Southern Biotech, USA and Molecular Probes (supplied by ThermoFisher, USA) respectively. A complete list of antibodies is provided in Table 1. PNGase F (P0704S) was from New England Biolabs (NEB), USA, Lipofectamine 3000 and Lipofectamine RNAiMax were from Invitrogen, USA. Dexamethasone (D1756) was from Sigma Aldrich, USA. siRNA against PrP (sc36318), and scrambled siRNA (sc37007) were from Santa Cruz Biotechnology, USA (sequences provided in Table 2).

Culture and characterization of human TM cells. Primary cultures of human TM cells were obtained from the Rhee laboratory and established from eye globes using the standard protocol^{35,62}, and characterized before by checking upregulation of myocilin in response to dexamethasone³⁵ (Supplementary Fig. S1a-b).

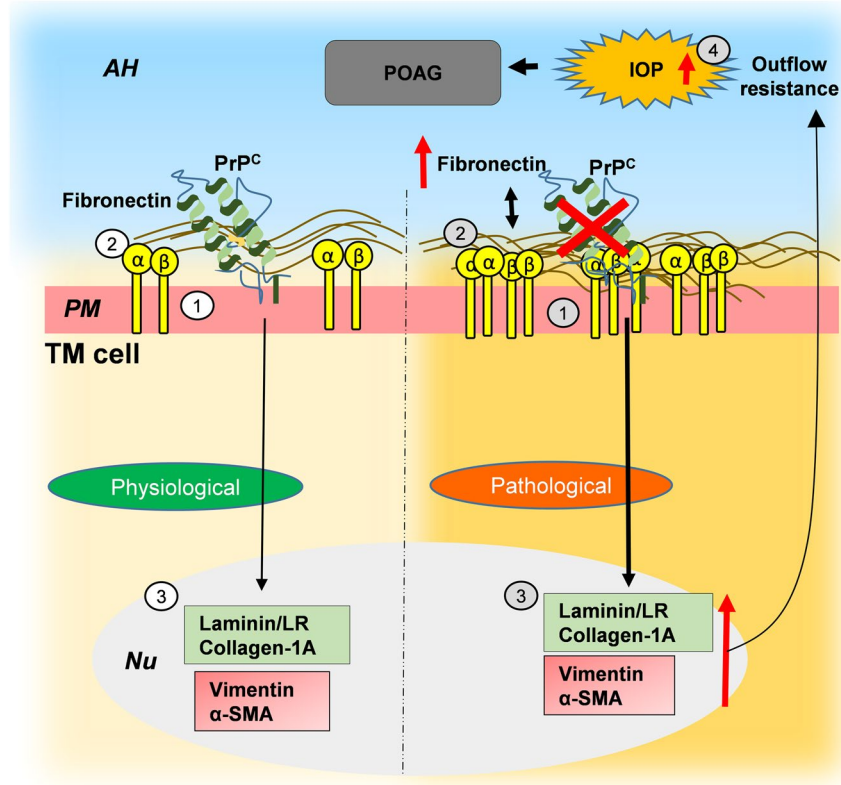


Figure 8. Hypothetical representation of PrP^C-mediated Endo-MT-like change in the TM. *Physiological role of PrP^C in the TM:* (1) PrP^C is expressed on the plasma membrane of TM cells. (2) PrP^C maintains cell-ECM interactions by stabilizing β 1-integrin and other proteins^{5,7}. *Pathological implications:* (1) Downregulation of PrP^C induces (2) aggregation of β 1-integrin and (3) upregulation of fibronectin, collagen 1A, α -SMA, vimentin, and laminin, resulting in (4) increase in IOP and possibly POAG. AH: aqueous humor; PM: plasma membrane; Nu: nucleus.

Primary human TM cell cultures were derived from several donors (age range: 56–78). After ciliary body (CB) was removed using scalpel, a cut in the rim of TM was made and the TM tissue was pulled out carefully using surgical grade forceps. Then, we made six sections of TM tissue using scalpel. Tissue sections were washed once in clean media and placed into the well of 6-wellplates. A coverslip was washed twice in clean media and placed gently over tissue sample keeping tissue sample toward center of well. Air bubbles were avoided during the whole process. The well was carefully handled in order not to scratch bottom of wells. Three milliliter of the media were added to each well dropping directly over the coverslip. The plate was incubated in 37 °C, 10% of CO₂ incubator. The growth of TM was checked for 3 weeks. Once the cells grew, media was replaced twice a week until cells grew confluent. TM cells were maintained in the growth medium consisted of Dulbecco's modified Eagle's medium (DMEM) supplemented with 20% fetal bovine serum (FBS) (Invitrogen-Gibco, Grand Island, NY), 1% L-glutamine (2 mM), and 0.5% or 0.1% gentamicin (50 or 10 μ g/mL). For further experiment, TM cultures were seeded into 6-well plates, allowed to grow to confluence at 37 °C in a 10% CO₂ atmosphere, and given an additional 2–3 days for differentiation. Confluent cultures of TM cells were used for all biochemical studies. For immunocytochemistry sub-confluent cultures were used to facilitate visualization of the plasma membrane. Both confluent and sub-confluent cultures responded to dexamethasone by upregulating myocilin (Supplementary Fig. S1c). To silence PrP^C, the cells were transfected with PrP-specific or the corresponding scrambled siRNA using Lipofectamine RNAiMax as per manufacturer's instructions. Desired downregulation of PrP^C was confirmed by Western blotting.

Human and bovine eye samples. Human eye globes were acquired from Lions Gift of Sight eye bank (1000 Westgate Dr Ste 260 Saint Paul, MN 55114). The donors ranged in age from 42–78 years. Other available details of donors are provided in Table 2. Bovine eyes were collected from a local abattoir. The samples were either fixed in buffered formalin (1:10) for immunohistochemistry, or dissected to isolate the desired tissues.

Mouse strains. PrP-knock out (PrP^{-/-}) mice were obtained from Jackson Laboratories (cat # 129-Prnptm2Edin/J Stock No: 012938) and crossed with C57BL/6 wild-type mice for 10 generations. F2 generation of wild type (PrP^{+/+}) and corresponding PrP^{-/-} (PrP^{-/-}) were used for these studies. Control and experimental mice were ~6 weeks old, sex matched, and maintained under similar conditions.

Antibody	Host species **	Species reactivity **	Company	Cat.No.	Dilution
PrP (3F4) IgG2a	m	h	Signet laboratories (Dedham, MA)	-	WB-1:250 IHC-1:50
PrP (8H4) IgG2b	m	m, h, b	Sigma Aldrich	P0110	WB-1:250 IHC-1:50
PrP (8B4) IgG ₁	m	m, h	Santa Cruz, USA	sc-47729	WB-1:250
PrP (SAF32) IgG2b	m	m, h, b	Cayman Chemical	189720	WB-1:250 IHC-1:50
PrP (G-12) IgG ₁	m	m, h	Santa Cruz, USA	sc-398451	WB-1:250
PrP (2301) IgG	Rb	h	<i>Gift by</i> Dr. Shu Chen, PhD	-	WB-1:500
Laminin receptor IgG	Rb	m, h	Abcam	ab137388	WB-1:1000 IHC-1:50
Alpha smooth muscle actin IgG2a	m	m, Rb, h, b	Abcam	ab7817	WB-1:2000 IHC-1:100
Laminin IgG	Rb	m, Rb, h,	Novus Biologicals	NB300-144	WB-1:1000 IHC-1:50
Fibronectin IgG1	m	h	Santa Cruz, USA	sc59826	WB-1:1000 IHC-1:50
Vimentin IgG1	m	h, b	Santa Cruz, USA	sc32322	WB-1:500 IHC-1:50
Myocilin IgG2b	m	h	Santa Cruz, USA	sc137233	WB-1:500 IHC-1:50
9EG7 anti activated β 1 integrin IgG2a	r	m, h	BD Biosciences	553715	ICC- 1:50 WB-1:500
Collagen 1A IgG	Rb	h, b	Rockland antibodies and assays	600-401-103-0.1	WB-1:500 IHC-1:50
β -actin IgG2b _κ	m	All species with actin	Millipore, USA	MAB1501	WB-1:5000
Mouse IgG - Control			Abcam	ab37355	IHC: 1:100
Rabbit IgG, Control			Abcam	ab37415	IHC: 1:100

Table 1. List of antibodies. **m: mouse, Rb: rabbit, b: bovine, h: human, r: rat.

PMI (h)/PCoD	Age (year)	Gender	Tissue region
Human tissues used for primary TM cell culture and whole tissue lysates Source: Lions Gift of Sight			
14	77	F	Trabecular meshwork/Retina
4.5	70	F	Trabecular meshwork/Retina/Optic nerve/Ciliary body
16/Dementia	69	M	Trabecular meshwork/Retina/Optic nerve/Ciliary body
5.5/ESLD	56	M	Trabecular meshwork/Retina/Optic nerve/Ciliary body
3/ESRD	78	F	Trabecular meshwork/Retina
12/Multiple system failure	67	M	Trabecular meshwork/Retina
7.5/Acute cardiac event	65	M	Trabecular meshwork/Retina
			TM cells from Dr. Rhee's lab (from 8 different donors at passage 2).
Mouse strain			
Wild-type and PrP knockout	6 weeks/5M & 5F	C57BL/6	Trabecular meshwork/Anterior Chamber
Bovine samples			
Breed			Tissue region
Mixed	—	—	— Trabecular meshwork/Anterior Chamber
siRNA			
Name	Company	Cat.No.	Sequence
Scrambled siRNA	Santa Cruz	sc-37007	Sense: UUCUCCGAACGUGUCACGUtt Antisense: ACGUGACACGUUCGGAGAAtt
PrP siRNA (h) is a pool of 3 different siRNA duplexes	Santa Cruz	sc-36318	sc-36318A: Sense: GUGACUAUGAGGACCGUUAtt Antisense: UAACGGUCCUCAUAGUCACtt sc-36318B: Sense: GAGACCGACGUUAGAUGAtt Antisense: UCAUCUUAACGUCGGUCUCtt sc-36318C: Sense: GUUGAGCAGAUGUGUAUCAAtt Antisense: UGAUACACAUCUGCUCAACtt

Table 2. List of biological samples and siRNA used in this study.

Tissue preparation and Immunohistochemistry. Immunocytochemistry and immunohistochemistry were performed as described⁴³. In short, thin sections of formalin-fixed TM tissue or primary human TM cells cultured on coverslips were processed for immunoreaction with the desired primary antibody followed by Alexa Fluor-conjugated secondary antibody. The nuclei were stained with Hoechst (#33342, Invitrogen, USA). Stained specimens were mounted and imaged with Leica inverted microscope (DMI8). Each experiment was repeated 3–4 times, and a representative image from 10 different fields is shown. Images of control sections reacted with isotype specific irrelevant primary antibody or buffer are shown in respective figures. Additional care was taken to identify the trabecular meshwork area for all sections in all the 3 species and the H&E staining for all sections analyzed were carried out and provided in the respective figures.

SDS-PAGE and Western blotting. Protein lysates and aqueous humor were fractionated by SDS-PAGE and analyzed by Western blotting as described³⁰. For Collagen1A blotting, the samples were processed in a non-reducing and non-denaturing condition. Quantification of protein bands was performed by densitometry using UN-SCAN-IT gels (version6.1) software (Silk Scientific, USA) and ImageJ Software analyzed graphically using GraphPad Prism (Version 5.0) software (GraphPad Software Inc., USA) and Microsoft excel. Full-length blots are included in Supplementary Fig. S2.

IOP measurement. IOP was measured at the same time of day with TonoLab tonometer (Colonial Medical Supply; USA-Icare, Finland). Mice were anesthetized with ketamine/xylazine before the measurement, and six measurements were obtained for each eye per animal. Average of all values was used for analysis.

Statistical analysis. Quantification of protein bands was performed and presented as Mean \pm SEM of the indicated n. Level of significance was calculated by Two-way ANOVA between the control and experimental groups.

References

- Prusiner, S. B. A unifying role for prions in neurodegenerative diseases. *Science* **336**, 1511–1513 (2012).
- Baskakov, I. V. The many shades of prion strain adaptation. *Prion* **8** (2014).
- Ma, J. & Wang, F. Prion disease and the 'protein-only hypothesis'. *Essays in biochemistry* **56**, 181–191, <https://doi.org/10.1042/bse0560181> (2014).
- Singh, N. *The Role of Iron in Prion Disease and Other Neurodegenerative Diseases*. Vol. 10 (2014).
- Alleaume-Butaux, A. *et al.* Double-Edge Sword of Sustained ROCK Activation in Prion Diseases through Neuritogenesis Defects and Prion Accumulation. *PLoS Pathog* **11**, e1005073, <https://doi.org/10.1371/journal.ppat.1005073> (2015).
- Zhong, Z. *et al.* Prion-like protein aggregates exploit the RHO GTPase to cofilin-1 signaling pathway to enter cells. *EMBO J* **37**, <https://doi.org/10.15252/embj.201797822> (2018).
- Kim, H. J. *et al.* Regulation of RhoA activity by the cellular prion protein. *Cell Death Dis* **8**, e2668, <https://doi.org/10.1038/cddis.2017.37> (2017).
- Loubet, D. *et al.* Neuritogenesis: the prion protein controls beta1 integrin signaling activity. *FASEB J* **26**, 678–690, <https://doi.org/10.1096/fj.11-185579> (2012).
- Martins, V. R. *et al.* Prion protein: orchestrating neurotrophic activities. *Current issues in molecular biology* **12**, 63 (2010).
- Lima, F. R. *et al.* Cellular prion protein expression in astrocytes modulates neuronal survival and differentiation. *J Neurochem* **103**, 2164–2176, <https://doi.org/10.1111/j.1471-4159.2007.04904.x> (2007).
- Mehrabian, M., Ehsani, S. & Schmitt-Ulms, G. An emerging role of the cellular prion protein as a modulator of a morphogenetic program underlying epithelial-to-mesenchymal transition. *Front Cell Dev Biol* **2**, 53, <https://doi.org/10.3389/fcell.2014.00053> (2014).
- Abu-Hassan, D. W., Acott, T. S. & Kelley, M. J. The trabecular meshwork: a basic review of form and function. *Journal of ocular biology* **2** (2014).
- Rao, P. V., Pattabiraman, P. P. & Kocczynski, C. Role of the Rho GTPase/Rho kinase signaling pathway in pathogenesis and treatment of glaucoma: Bench to bedside research. *Exp Eye Res* **158**, 23–32, <https://doi.org/10.1016/j.exer.2016.08.023> (2017).
- Pattabiraman, P. P., Maddala, R. & Rao, P. V. Regulation of plasticity and fibrogenic activity of trabecular meshwork cells by Rho GTPase signaling. *J Cell Physiol* **229**, 927–942, <https://doi.org/10.1002/jcp.24524> (2014).
- Braunger, B. M., Fuchshofer, R. & Tamm, E. R. The aqueous humor outflow pathways in glaucoma: A unifying concept of disease mechanisms and causative treatment. *Eur J Pharm Biopharm* **95**, 173–181, <https://doi.org/10.1016/j.ejpb.2015.04.029> (2015).
- Weinreb, R. N., Aung, T. & Medeiros, F. A. The pathophysiology and treatment of glaucoma: a review. *JAMA* **311**, 1901–1911, <https://doi.org/10.1001/jama.2014.3192> (2014).
- Tanna, A. P. & Johnson, M. Rho Kinase Inhibitors as a Novel Treatment for Glaucoma and Ocular Hypertension. *Ophthalmology* **125**, 1741–1756, <https://doi.org/10.1016/j.ophtha.2018.04.040> (2018).
- Torrejon, K. Y. *et al.* TGFbeta2-induced outflow alterations in a bioengineered trabecular meshwork are offset by a rho-associated kinase inhibitor. *Sci Rep* **6**, 38319, <https://doi.org/10.1038/srep38319> (2016).
- Garamszegi, N. *et al.* Extracellular matrix-induced transforming growth factor-beta receptor signaling dynamics. *Oncogene* **29**, 2368–2380, <https://doi.org/10.1038/onc.2009.514> (2010).
- Gagen, D., Faralli, J. A., Filla, M. S. & Peters, D. M. The role of integrins in the trabecular meshwork. *J Ocul Pharmacol Ther* **30**, 110–120, <https://doi.org/10.1089/jop.2013.0176> (2014).
- Mamuya, F. A. & Duncan, M. K. aV integrins and TGF-beta-induced EMT: a circle of regulation. *J Cell Mol Med* **16**, 445–455, <https://doi.org/10.1111/j.1582-4934.2011.01419.x> (2012).
- Montecchi-Palmer, M. *et al.* TGFbeta2 Induces the Formation of Cross-Linked Actin Networks (CLANs) in Human Trabecular Meshwork Cells Through the Smad and Non-Smad Dependent Pathways. *Invest Ophthalmol Vis Sci* **58**, 1288–1295, <https://doi.org/10.1167/iovs.16-19672> (2017).
- Honjo, M. *et al.* Role of the Autotaxin-LPA Pathway in Dexamethasone-Induced Fibrotic Responses and Extracellular Matrix Production in Human Trabecular Meshwork Cells. *Invest Ophthalmol Vis Sci* **59**, 21–30, <https://doi.org/10.1167/iovs.17-22807> (2018).
- Takahashi, E., Inoue, T., Fujimoto, T., Kojima, S. & Tanihara, H. Epithelial mesenchymal transition-like phenomenon in trabecular meshwork cells. *Exp Eye Res* **118**, 72–79, <https://doi.org/10.1016/j.exer.2013.11.014> (2014).
- Munger, J. S. & Sheppard, D. Cross talk among TGF-beta signaling pathways, integrins, and the extracellular matrix. *Cold Spring Harb Perspect Biol* **3**, a005017, <https://doi.org/10.1101/cshperspect.a005017> (2011).
- Ghodrati, F. *et al.* The prion protein is embedded in a molecular environment that modulates transforming growth factor beta and integrin signaling. *Sci Rep* **8**, 8654, <https://doi.org/10.1038/s41598-018-26685-x> (2018).
- Sharma, S. *et al.* Proteomic Alterations in Aqueous Humor From Patients With Primary Open Angle Glaucoma. *Invest Ophthalmol Vis Sci* **59**, 2635–2643, <https://doi.org/10.1167/iovs.17-23434> (2018).

28. Gil, M. *et al.* Cellular prion protein regulates invasion and migration of breast cancer cells through MMP-9 activity. *Biochem Biophys Res Commun* **470**, 213–219, <https://doi.org/10.1016/j.bbrc.2016.01.038> (2016).
29. Gauthier, A. C. & Liu, J. Epigenetics and Signaling Pathways in Glaucoma. *Biomed Res Int* **2017**, 5712341, <https://doi.org/10.1155/2017/5712341> (2017).
30. Ashok, A. *et al.* Prion protein modulates iron transport in the anterior segment: Implications for ocular iron homeostasis and prion transmission. *Experimental eye research* (2018).
31. Gu, Y. *et al.* Mutant prion protein-mediated aggregation of normal prion protein in the endoplasmic reticulum: implications for prion propagation and neurotoxicity. *Journal of neurochemistry* **84**, 10–22 (2003).
32. Yang, C.-Y. C., Huynh, T., Johnson, M. & Gong, H. Endothelial glycocalyx layer in the aqueous outflow pathway of bovine and human eyes. *Experimental eye research* **128**, 27–33 (2014).
33. Altmeppen, H. C. *et al.* Proteolytic processing of the prion protein in health and disease. *Am J Neurodegener Dis* **1**, 15–31 (2012).
34. Fujimoto, T. *et al.* Involvement of RhoA/Rho-associated kinase signal transduction pathway in dexamethasone-induced alterations in aqueous outflow. *Invest Ophthalmol Vis Sci* **53**, 7097–7108, <https://doi.org/10.1167/iops.12-9989> (2012).
35. Keller, K. E. *et al.* Consensus recommendations for trabecular meshwork cell isolation, characterization and culture. *Exp Eye Res* **171**, 164–173, <https://doi.org/10.1016/j.exer.2018.03.001> (2018).
36. Nuvolone, M., Sorce, S., Paolucci, M. & Aguzzi, A. Extended characterization of the novel co-isogenic C57BL/6J Prnp^{-/-} mouse line. *Amyloid: the international journal of experimental and clinical investigation: the official journal of the International Society of Amyloidosis* **24**, 36–37, <https://doi.org/10.1080/13506129.2017.1289913> (2017).
37. Nuvolone, M. *et al.* Strictly co-isogenic C57BL/6J-Prnp^{-/-} mice: A rigorous resource for prion science. *The Journal of experimental medicine* **213**, 313–327, <https://doi.org/10.1084/jem.20151610> (2016).
38. Acott, T. S. & Kelley, M. J. Extracellular matrix in the trabecular meshwork. *Experimental eye research* **86**, 543–561, <https://doi.org/10.1016/j.exer.2008.01.013> (2008).
39. Chen, S. G. *et al.* Truncated forms of the human prion protein in normal brain and in prion diseases. *Journal of Biological Chemistry* **270**, 19173–19180 (1995).
40. Watt, N. T. *et al.* Reactive oxygen species-mediated beta-cleavage of the prion protein in the cellular response to oxidative stress. *J Biol Chem* **280**, 35914–35921, <https://doi.org/10.1074/jbc.M507327200> (2005).
41. Altmeppen, H. C. *et al.* Roles of endoproteolytic alpha-cleavage and shedding of the prion protein in neurodegeneration. *FEBS J* **280**, 4338–4347, <https://doi.org/10.1111/febs.12196> (2013).
42. Lewis, V. *et al.* Prion protein “gamma-cleavage”: characterizing a novel endoproteolytic processing event. *Cell Mol Life Sci* **73**, 667–683, <https://doi.org/10.1007/s00018-015-2022-z> (2016).
43. Ashok, A. & Singh, N. Prion protein modulates glucose homeostasis by altering intracellular iron. *Scientific reports* **8** (2018).
44. Asthana, A. *et al.* Prion protein facilitates retinal iron uptake and is cleaved at the β -site: Implications for retinal iron homeostasis in prion disorders. *Scientific reports* **7**, 9600 (2017).
45. Linsenmeier, L. *et al.* Diverse functions of the prion protein - Does proteolytic processing hold the key? *Biochim Biophys Acta Mol Cell Res* **1864**, 2128–2137, <https://doi.org/10.1016/j.bbamcr.2017.06.022> (2017).
46. Garcia-Castineiras, S. Iron, the retina and the lens: a focused review. *Experimental eye research* **90**, 664–678, <https://doi.org/10.1016/j.exer.2010.03.003> (2010).
47. Mays, C. E. *et al.* Endoproteolytic processing of the mammalian prion glycoprotein family. *The FEBS journal* **281**, 862–876 (2014).
48. McDonald, A. J. & Millhauser, G. L. PrP overdrive: Does inhibition of α -cleavage contribute to PrPC toxicity and prion disease? *Prion* **8**, 183–191 (2014).
49. Haigh, C. L. & Collins, S. J. Endoproteolytic cleavage as a molecular switch regulating and diversifying prion protein function. *Neural regeneration research* **11**, 238 (2016).
50. McDonald, A. J., Dibble, J. P., Evans, E. G. & Millhauser, G. L. A new paradigm for enzymatic control of α -cleavage and β -cleavage of the prion protein. *Journal of Biological Chemistry* **289**, 803–813 (2014).
51. Jarosz-Griffiths, H. H. *et al.* Proteolytic shedding of the prion protein via activation of metallopeptidase ADAM10 reduces cellular binding and toxicity of amyloid- β oligomers. *Journal of Biological Chemistry* **294**, 7085–7097 (2019).
52. Altmeppen, H. C. *et al.* The shedase ADAM10 is a potent modulator of prion disease. *Elife* **4**, e04260 (2015).
53. Taylor, D. R. *et al.* Role of ADAMs in the ectodomain shedding and conformational conversion of the prion protein. *Journal of Biological Chemistry* **284**, 22590–22600 (2009).
54. Linsenmeier, L. *et al.* Structural and mechanistic aspects influencing the ADAM10-mediated shedding of the prion protein. *Mol Neurodegener* **13**, 18, <https://doi.org/10.1186/s13024-018-0248-6> (2018).
55. Noy, P. J. *et al.* TspanC8 Tetraspanins and A Disintegrin and Metalloprotease 10 (ADAM10) Interact via Their Extracellular Regions: EVIDENCE FOR DISTINCT BINDING MECHANISMS FOR DIFFERENT TspanC8 PROTEINS. *J Biol Chem* **291**, 3145–3157, <https://doi.org/10.1074/jbc.M115.703058> (2016).
56. De Groef, L., Van Hove, I., Dekeyster, E., Stalmans, I. & Moons, L. MMPs in the trabecular meshwork: promising targets for future glaucoma therapies? *Investigative ophthalmology & visual science* **54**, 7756–7763 (2013).
57. Haigh, C. L. *et al.* Dominant roles of the polybasic proline motif and copper in the PrP23–89-mediated stress protection response. *Journal of cell science* **122**, 1518–1528 (2009).
58. Pattabiraman, P. P. & Rao, P. V. Mechanistic basis of Rho GTPase-induced extracellular matrix synthesis in trabecular meshwork cells. *American Journal of Physiology-Cell Physiology* (2009).
59. Richardson, D. D. *et al.* The prion protein inhibits monocytic cell migration by stimulating beta1 integrin adhesion and uropod formation. *J Cell Sci* **128**, 3018–3029, <https://doi.org/10.1242/jcs.165365> (2015).
60. Ezepeleta, J. *et al.* Protective role of cellular prion protein against TNF α -mediated inflammation through TACE α -secretase. *Scientific reports* **7**, 7671 (2017).
61. Alleaume-Butaux, A. *et al.* Cellular prion protein is required for neuritogenesis: fine-tuning of multiple signaling pathways involved in focal adhesions and actin cytoskeleton dynamics. *Cell Health and Cytoskeleton* **5**, 1–12 (2013).
62. Oh, D.-J. *et al.* Overexpression of SPARC in Human Trabecular Meshwork Increases Intraocular Pressure and Alters Extracellular Matrix SPARC Overexpression Increases IOP and TM ECM. *Investigative ophthalmology & visual science* **54**, 3309–3319, <https://doi.org/10.1167/iops.12-11362> (2013).

Acknowledgements

Funded by R01 NS 092145 to NS.

Author Contributions

A.A.: planned and performed all experiments, analyzed the data, wrote and modified the manuscript; N.S.: conceived the idea, overlooked experimental design, analyzed the data, wrote the manuscript; M.H.K.: harvested and cultured primary human T.M. cells, provided feedback; A.S.W.: performed de-glycosylation and Western blotting; W.M.J.: provided reagents and feedback; M.L.: cultured T.M. cells and performed immunohistochemistry; R.R.: assisted in Western blot analysis; D.R. and P.P.: provided feedback.

Additional Information

Supplementary information accompanies this paper at <https://doi.org/10.1038/s41598-019-49482-6>.

Competing Interests: The authors declare no competing interests.

Publisher's note: Springer Nature remains neutral with regard to jurisdictional claims in published maps and institutional affiliations.



Open Access This article is licensed under a Creative Commons Attribution 4.0 International License, which permits use, sharing, adaptation, distribution and reproduction in any medium or format, as long as you give appropriate credit to the original author(s) and the source, provide a link to the Creative Commons license, and indicate if changes were made. The images or other third party material in this article are included in the article's Creative Commons license, unless indicated otherwise in a credit line to the material. If material is not included in the article's Creative Commons license and your intended use is not permitted by statutory regulation or exceeds the permitted use, you will need to obtain permission directly from the copyright holder. To view a copy of this license, visit <http://creativecommons.org/licenses/by/4.0/>.

© The Author(s) 2019